RESEARCH PAPER
Contrib. Sci. & Tech Eng, 2025, 2(1)
Homepage: https://cste.journals.umz.ac.ir/
DOI: 10.22080/cste.2025.28906.1024

A Framework for Alzheimer's Disease Diagnosis Using Dempster-Shafer Theory and Multimodal MRI Fusion of White and Gray Matter

Fatemeh Bahadoran [1], Jamal Ghasemi [2]*

[1] *Babol University of Medical Sciences, Mazandaran, Iran.*

[2] *Faculty of Engineering & Technology, University of Mazandaran, Babolsar, Iran.*

Article Info
Received 17 February 2025
Accepted 30 March 2025
Available online 30 March 2025

Keywords:
Alzheimer's Disease;
MRI, Uncertainty;
CAD System;
Dempster-Shafer Theory;
Evidence Theory;
Mass Function.

Abstract:
Alzheimer's disease (AD) is a common neurodegenerative disorder that requires early diagnosis for effective treatment. MRI data provides valuable insights into brain structure, which can assist in diagnosing the disease. However, traditional diagnostic methods often face errors due to expert limitations and data uncertainty. To address this issue, we propose a Computer-Aided Diagnosis (CAD) system that can automatically identify the disease. Moreover, since MRI images inherently contain uncertainty, the proposed method offers a solution to minimize this uncertainty. In the proposed method, the information obtained from brain white matter (WM) and gray matter (GM) is combined after performing preprocessing, feature extraction, and selection steps. This combination is achieved using the Evidence Theory and Dempster-Shafer Theory (DST). In this theory, mass functions are employed instead of probability functions. Subsequently, three different classifiers are applied separately in the final stage to the combined data. Experimental results demonstrate that combining GM and WM data using DST achieves higher accuracy compared to using either data type alone. This fusion-based method presents a reliable and effective approach for improving Alzheimer's diagnosis. Our proposed method achieved 91% accuracy in three different binary classification cases using the LDA classifier when distinguishing between AD and Normal Control (NC) groups. This result, obtained by combining WM and GM data, demonstrated a significant improvement compared to using each data type independently.

***Corresponding Author:** j.ghasemi@umz.ac.ir

Supplementary information: Supplementary information for this article is available at https://cste.journals.umz.ac.ir/

Please cite this paper as: Bahodoran, F., & Ghasemi, J. (2025). A Framework for Alzheimer's Diagnosis Using Dempster-Shafer Theory and Multimodal MRI Fusion of White and Gray Matter. Contributions of Science and Technology for Engineering, 2(1), 28-36. doi:10.22080/cste.2025.28906.1024.

1. Introduction

Alzheimer's disease (AD) is the most common cause of dementia [1]. This disease leads to memory impairment and loss of mental ability. There is currently no treatment for Alzheimer's disease [2], but an early diagnosis of this disease can reduce its speed of progression. One of the methods for diagnosing this disease, is using the images obtained through various medical imaging methods such as MRI.

The analysis of the images obtained through methods such as MRI by a physician or a specialist is extremely fallible due to the large volume of data. In addition, MRI images are images with an element of uncertainty [3], which is caused by various factors, such as the effect of the partial volumes and noise. Hence, introducing a computer-aided diagnosis (CAD) system that can measure the changes in the brain following the onset of Alzheimer's disease is helpful.

In general, a CAD system that diagnoses Alzheimer's disease based on MRI has four main steps. In step one, the input data (MRI images) is received. Preprocessing is performed in the second step to facilitate coordination between different individuals' brains and to compare different groups. In step three, the features and sizes are obtained from the resulting images, and in the final step, classification is carried out to identify Alzheimer's disease in the input data [4].

In this regard, in some studies, Alzheimer's disease was identified through the measurements of brain structures such as the entorhinal cortex (EC) and right and left amygdalae [5].

A structure such as the entorhinal cortex is not enough to diagnose Alzheimer's, and the use of a set of structures can improve the diagnosis accuracy. Hence, various studies were carried out based on the brain white matter and gray matter density maps. These studies extracted features on the voxel level using methods such as VBM and used them to diagnose Alzheimer's disease [6-8].

*ISSN **3060-6578***

Since the more realistic CAD system is the most favorable, uncertainty modeling in a CAD system can improve system efficiency. Data fusion is one of the uncertainty modeling methods. Moreover, there are various data fusion methods, including the evidence theory. The evidence theory has been used for data fusion in numerous studies [9-11]. This theory is also utilized in studies on Alzheimer's disease [12].

The rest of this paper is arranged as follows: In section two, the research literature, tools, and materials are introduced. The third section describes the proposed method. The fourth section also presents the tables of the results and the analyses. Finally, the paper ends with the conclusion section.

2. Materials and Methods

2.1. Database

Data used in this study was obtained from the ADNI database(http://www.loni.ucla.edu/ADNI), which is a part of the LONI IDA user environment [13]. The participants in this project, which was launched in 2004, included patients with Alzheimer's disease and MCI and healthy individuals from North America [14]. This research database includes three groups: AD, CN, which is considered a controlled normal or healthy group, and MCI groups. In fact, MCI could be considered the middle stage between aging and dementia, including Alzheimer's disease. The group classification of this data is also carried out based on the CDR and MMSE scores gained by the participants.

The research data in this paper are obtained from sMRI images with a weight of T1 and the ADNI1-Screening research phase. Moreover, 600 participants took part in this study. Table 1, presents the study data specifications.

Table 1. Demographic data of patients in the database (ADNI 1075-T1)

Diagnosis	Number	Gender(M/F)	MMSE
AD	200	96/104	29 ± 1
MCI	200	80/120	26 ± 2
CN	200	100/100	23 ± 2

In the LONI database, the MRI images are exposed to three pre-processing steps [15]. These steps include: Grad Warp, B1 non-uniformity, and N3[16].

2.2. Feature Extraction (Principal Component Analysis)

PCA (Principal Component Analysis) [17] is a method for downsizing and extracting the best data features so that fewer features represent all features. PCA is, in fact, a method in which the inputs are mapped to a new space using a rotation matrix. Data scattering increases in the transformed space. This method is also used to analyze neurological images to reduce the image dimensional space [18].

Assume X represents the input instances, such that N shows the number of data and m is the dimensional space. In fact, matrix X is a $m \times N$ matrix.

$$X = [x_1, x_2, \ldots, x_N]; \qquad X \in lR^m \tag{1}$$

The mean of data also has to be zero.

$$E\{X\} = \frac{1}{N}\sum_{i=1}^{N} X_i = 0; \tag{2}$$

However, if this condition is not met, the resulting mean of the data has to be subtracted from each individual data point. As a result, the input vectors are normalized.

A rotation matrix is needed to rotate the axes and enter a new feature space. The rotation matrix is obtained by obtaining the covariance matrix of the input data and the eigenvalues and eigenvectors using this matrix. To this end, the covariance matrix of input data is calculated via Equation 3:

$$\sum X = \frac{1}{N}\sum_{i=1}^{N} x_i x_i^T = \frac{1}{N} XX^T \tag{3}$$

The covariance matrix is square, and its value is assumed to equal R. In this case, the eigenvalues and eigenvectors of the covariance matrix are obtained via Equation 4:

$$Rq = \lambda q \tag{4}$$

In the equation above, q denotes the eigenvector and λ represents the eigenvalue. In this equation, there is a q value corresponding to each λ value. Eigenvectors are obtained when the λ values are sorted descending, and the eigenvectors corresponding to each λ are obtained. A new space is obtained by multiplying the λ values by the input data, which offers the highest data resolution.

XX^T is a $m \times m$ matrix, where m denotes the size of each input data and equals 121×145×121. Besides, $X^T X$ is a $N \times N$ matrix (N show the number of instances) .If the size of N is considerably smaller than m, it is possible to reduce computational complexity by using the diagonalizing $X^T X$ instead of XX^T [19].

Let v_i show the eigenvectors of matrix XX^T, which is obtained as follow:

$$X^T X v_i = \mu_i v_i \tag{5}$$

Equation 6 is obtained by multiplying the two sides of the Equation 5 by matrix X:

$$XX^T X v_i = \mu_i X v_i \tag{6}$$

In this equation, Xv_i shows the $\sum X = XX^T$ eigenvectors. The size of the $L = X^T X$ matrix is $N \times N$, where $L_i^j = X_i^T X_j$ and the v_l eigenvectors are calculated using L. These vectors are identified as u_l Eigen Brains using a linear composition of N image sets [20, 21].

$$u_l = \sum_{k=1}^{N} v_{lk} x_k \tag{7}$$

2.3. Classifier

In machine learning classification methods, the goal is to identify the input patterns and instances with the aim of classifying the input instance into a class, which is considered the best class for the given instance as compared to the other classes. Bayes' theorem [22] uses the most probable class approach for the classification of the input data to attain this goal.

The NBC (Naive Bayesian Classification) classifier is a classifier that follows Bayes' theorem [23]. In this classifier, it is assumed all the variables that are involved in this classification are independent pair-wise [24]. To calculate probability, it is enough to use the joint probability. It is reduced based on the independence of the variables and components using conditional probability.

In addition to NBC, QDA and LDA is also a classifier of the DA (Discriminant Analysis) family, which follows the Bayesian rule. DA was originally introduced by Geisser (1964) and Keehn(1965) based on Bayesian estimations [25]. The decision boundary in the QDA classifier is nonlinear [26].

2.4. Evidence Theory

Dempster-Shafer's theory (DST), or the evidence theory, is an extended version of the classical probability theory [27]. This theory, is a flexible and effective mathematical tool for presenting and combining ignorant information [27, 28]. In the evidence theory, it is assumed a universal set of mutually exclusive elements known as the Frame Of Discernment (FOD) is written as $\Omega = \{\theta_1, \theta_2, \theta_3, \ldots, \theta_n\}$. Each Ω subset can be interpreted as a possible answer to a question. In addition, only one of these subsets is correct for each question. The frame of discernment (FOD) power set (2^{Ω}) consists of elements that contain the answer to all the questions possibly raised in the frame of discernment. The evidence theory defines three important functions: the Basic Probability Assignment (BPA) or the Mass Function, the Belief Function, and the Plausibility Function.

The mass function, which is denoted by μ, shows the degree of the belief of a witness in a subject. The mass function is a map of the power set of the frame of discernment with a closed interval of 0 and 1. Therefore, the mass of the empty element is zero and the sum of the masses equals one. In other words:

$$\mu: 2^{\Omega} \rightarrow [0,1] \quad \text{where } \mu(\emptyset) = 0 \ \& \ \Sigma_{i \subseteq \Omega} \mu(A) = 1 \tag{8}$$

The sum of the masses (the allocated basic probabilities) of all sets like B that meet condition 8 forms the belief of set A, Equation 9. The belief of set A forms the lower boundary of the uncertainty interval, which includes the exact probability of the given set (with regard to classical probability) [27, 29].

$$Bel(A) = \sum_{B|B \subseteq A} \mu(B), Bel(\emptyset) = 0, Bel(\Omega) = 1 \tag{9}$$

One of the important advantages of the evidence theory is its ability to combine belief structures. The result of this combination generally reduces the belief uncertainty range. Since this advantage leads to the development of a model that contains the opinions of all the witnesses, it is substantially important. Dempster's rule of combination is a method for combining the mass functions of the independent resources on a frame of discernment based on the orthogonal sum of the mass functions. Consider two belief structures with mass functions $\mu_1$and μ_2. Function μ_{12} is the orthogonal sum of two belief structures and it is denoted by $(\mu_1 \oplus \mu_2)$. Besides, μ_1 is calculated as follows, using Dempster's rule of combination:

$$\mu_{12}(A) = \frac{\sum_{B \cap C = A} \mu_1(B)\mu_2(C)}{1 - K_{12}} \quad A \neq \emptyset, \mu_{12}(\emptyset) = 0 \tag{10}$$

$$K_{12} = \sum_{B \cap C = \emptyset} \mu_1(B)\mu_2(C) \tag{11}$$

Since Dempster's rule of combination has two major advantages, namely commutativity and associativity [27], Equations 10 and 11 can be extended such that:

$$\mu_{12\ldots n}(A) = \frac{\sum_{A_1 \cap A_2 \ldots A_n = \emptyset} \mu_1(A_1)\mu_2(A_2)\ldots\mu_n(A_n)}{1 - K_{12\ldots n}} \quad A \neq \emptyset, \mu_{12\ldots n}(\emptyset) = 0 \tag{12}$$

$$K_{12\ldots n} = \sum_{A_1 \cap A_2 \ldots A_n = \emptyset} \mu_1(A_1)\, \mu_2(A_2) \ldots \mu_n(A_n) \tag{13}$$

The denominators in Equations 12 and 13, i.e. terms $1 - K_{12}$ and $1 - K_{12\ldots n}$, are called the normalization factors. Moreover, K_{12} indicates the degree of inconsistency of two belief structures, while two belief structures are combinable when $K_{12} \neq 1$. The Proposed Method

The block diagram in Figure 1 shows the CAD system proposed in this paper for the automated classification of Alzheimer's disease.

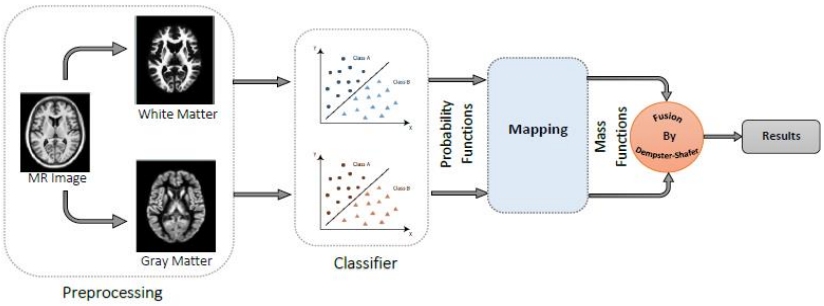

Figure 1. Block diagram of the proposed method.

Preprocessing is the first step in the CAD system. The MRI images used in this paper were preprocessed in SPM12 software using the DARTEL algorithm, indicating the diffeomorphic anatomical matching using Lie exponential algebra [30, 31]. In sum, the preprocessing steps taken in this paper are as follows: 1) first, reorientation is performed to change the position of the brain in each person for the approximate matching of the images to the standard space. It is registered using the 9-parameter affine transformation to the MNI space. 2) The next step involves automated segmentation. The results of this step are six images including images of the white matter, gray matter, cerebrospinal fluid, the hard tissue, the soft tissue around the brain, and the background image. The white matter and gray matter images are used in the next steps. 3) The rigidly aligned version of the segmented images of the white matter and gray matter obtained in the previous step, was generated. 4) The template was created, which is named DARTEL, and the obtained flow fields were applied to the modulated 3D T1-weighted images of single subjects (generated by the segmentation step) to warp them to the common DARTEL space and then modulated using the Jacobian determinants. 5) The modulated 3D T1-weighted images from DARTEL were normalized to the MNI template. In this stage, the size of all images in the 3-dimensional space is changed to $121 \times 145 \times 121$. 6)The last step in preprocessing involves smoothing using the 8-millimeter Gaussian kernel [31].

The computation load can be reduced by applying a mask. This mask is obtained by calculating the mean of all the tissue images of the healthy individuals and keeping the voxels that have intensities over 10% higher than the maximum intensity of the mean image; therefore, the size of each image matrix is decreased from 2122945 to 356733 and 564735 for the white matter and the gray matter tissue images, respectively. In the next step, features with the highest potential for differentiating between different classes are selected by applying PCA to the input data. Figures 2-a and 2-b, shows the data of the gray matter and white matter images using two PCA scores. Following the application of PCA, data classification is carried out using the QDA, LDA, and NBC classifiers. Finally, the information obtained from each classifier, applied separately to gray matter and white matter, is fused using evidence theory to minimize uncertainty and improve diagnostic reliability. As for the current problem, the goal is to identify and decide on the data considering the two selected classes. In this study, three two-class categories, namely $\{AD, CN\}$, $\{AD, MCI\}$, and $\{MCI, CN\}$, are used. In this study, the probability functions generated by each classifier for both white matter and gray matter are converted into mass functions based on evidence theory.

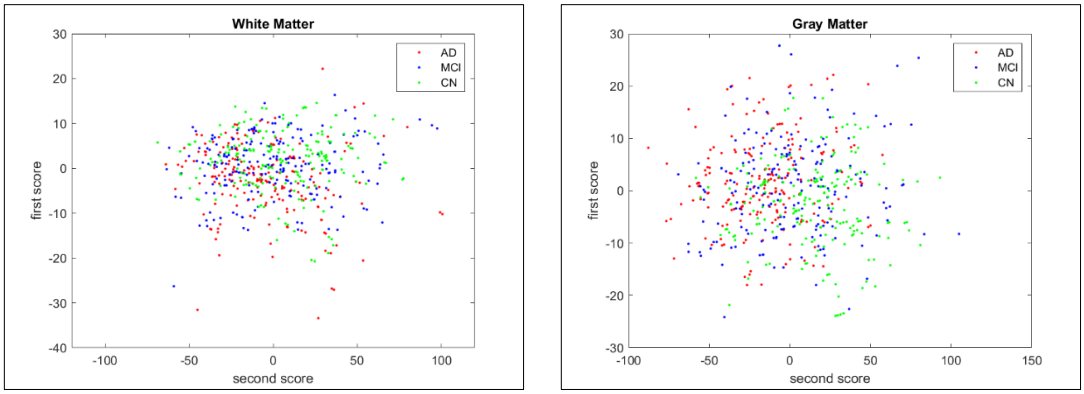

(a) (b)

Figure 2. Representation of all data using only the two first Scores of PCA: (a) White matter; (b) Gray matter.

The value allocated to the nonexclusive (indefinite) mass in the current space is defined by the distance between the probabilities of two propositions $(\{AD, CN\}, \{AD, MCI\}, \{MCI, CN\})$. In fact this conversion is performed using a thresholding process, where the distance between two propositions serves as the thresholding mechanism. Three states are defined for the size of the distance between these two propositions: the perfect uncertainty (PU), semi-uncertainty (SU), and no uncertainty (NU) state [32]. The following explanation illustrates this conversion process:

The distance between two probabilities allocated to two propositions is shown by α. The probability values allocated to the first and second classes are denoted by P_1 and P_2, respectively. Moreover, the mass sizes allocated to the first, the second, and common classes shared by the first and second classes are shown by m_1, m_2, and m_{12}, respectively. Therefore, the three states are defined as follows:

1) The alpha for values greater than or equal to 0.8 ($\alpha \geq 0.8$):

This state is considered the NU (No Uncertainty) state wherein:

$$\begin{cases} m_1 = p_1 \\ m_2 = p_2 \\ m_{12} = 0 \end{cases} \quad (14)$$

2) The alpha for values between 0.8 and 0.2 ($0.8 < \alpha < 0.2$):

This state is considered the SU (Semi Uncertainty) state wherein:

$$p_1 < p_2 \& \lambda = \frac{p_1}{p_2} \; where \begin{cases} m_1 = p_1 - \frac{\lambda}{2} \\ m_2 = p_2 - \frac{\lambda}{2} \\ m_{12} = \lambda \end{cases} \quad (15)$$

3) The alpha for values less than or equal to 0.2 ($\alpha \leq 0.8$) :

This state is considered the PU (Perfect Uncertainty) state wherein:

$$\begin{cases} m_1 = \frac{p_1}{2} \\ m_2 = \frac{p_2}{2} \\ m_{12} = \frac{p_1 + p_2}{2} \end{cases} \quad (16)$$

Subsequently, the mass functions obtained from the classifications of both matter types are fused to enhance diagnostic accuracy and reduce uncertainty. This fusion process leads to improved results as it combines the insights derived from two distinct data sources, providing a more comprehensive and reliable diagnosis.

3. Results

The system's performance proposed in this study is estimated using the k-fold method. In the k-fold method, data is randomly and equally divided into k separate subsets and training and testing are carried out k times [33]. In this study, k is set to 5, and 160 training data and 40 testing data are allocated to each training round to validate the model.

The effectiveness of a CAD system is assessed with regard to the accuracy criterion. In addition to accuracy, specificity and sensitivity are the other criteria for assessing the system's performance. Accuracy, specificity, and sensitivity are defined as follows:

$$ACC = \frac{TP+TN}{TP+TN+FP+FN}$$
$$SENS = \frac{TP}{TP+FN} \quad (17)$$
$$SPEC = \frac{TN}{TN+FP}$$

This study was conducted separately for each classifier, and the results were classified into two classes.

3.1. Classification Using Bayesian Classifier

Figures 3-a to 3-c, are the accuracy values corresponding to each PCA component for both binary classification scenarios and when using the Bayesian classifier. Based on the figure, we can observe that for most PCA components and across all three binary classification scenarios, combining the WM and GM output results yields higher accuracy compared to using WM or GM alone. The results presented in Table 2 show the accuracy values for three binary states using five PCA components when white matter, gray matter, and their combinations are used.

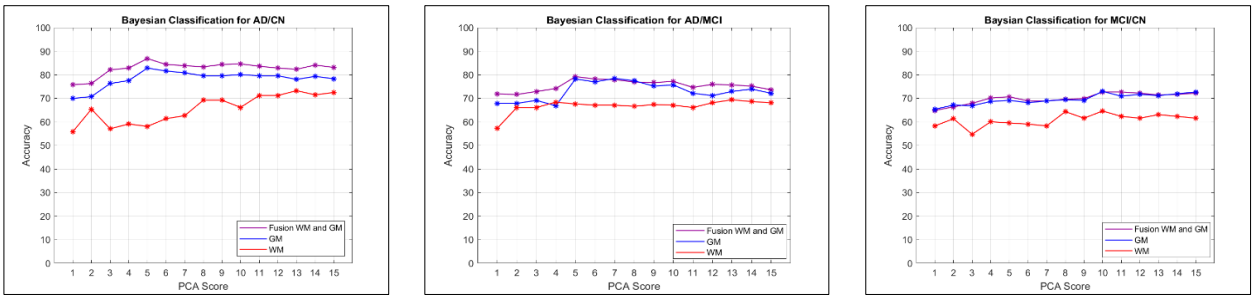

(a) (b) (c)

Figure 3. The accuracy values for the three binary classification cases were determined using white matter (red color), gray matter (blue color), and the proposed method (purple color) for 15 PCA components with Bayesian as the classifier.

Table 2. Sensitivity, accuracy, and specificity values (%) of WM, GM, and the proposed method for five components of PCA and three two-class states while using Bayesian as a classifier.

GROUPS	ACC			SPEC			SENS		
	WM	GM	Proposed Method	WM	GM	Proposed Method	WM	GM	Proposed Method
AD/CN	58	82	87	48	78	81	66	88	90
AD/MCI	68	78	79	63	72	72	72	81	84
MCI/CN	59	70	71	57	66	66	60	72	75

The proposed method's accuracy in classifying groups CN and AD was 87%, while it was 79% and 71% in the two-class AD/MCI and MCI/CN states. In classifying groups AD and CN, the proposed method improved approximately 6% and 29% compared to using gray matter and white matter alone, respectively.

3.2. Classification Using DA(Quadratic and Linear) Classifier

Tables 3 and 4 present the results obtained from applying the LDA and QDA classifiers for white matter, gray matter, and the proposed method using 5 PCA components. By observing these results, we can infer and conclude that the

classifiers mentioned have also demonstrated satisfactory performance in disease detection for all three binary classification cases. Figures 4 and 5 also present the accuracy values for 15 PCA components for both classifiers. From the figures, it can be observed that the proposed method can lead to improved accuracy by fusing and combining white matter and gray matter data.

Table 3. Sensitivity, accuracy, and specificity values (%) of WM, GM, and the proposed method for five components of PCA and three two-class states while using LDA as a classifier.

GROUPS	ACC			SPEC			SENS		
	WM	GM	Proposed Method	WM	GM	Proposed Method	WM	GM	Proposed Method
AD/CN	69	83	91	66	82	88	72	85	94
AD/MCI	68	81	82	64	79	78	73	82	85
MCI/CN	66	72	73	63	70	67	73	75	79

Table 4. Sensitivity, accuracy, and specificity values(%) of WM, GM, and the proposed method for five components of PCA and three two-class states while using QDA as a classifier.

GROUPS	ACC			SPEC			SENS		
	WM	GM	Proposed Method	WM	GM	Proposed Method	WM	GM	Proposed Method
AD/CN	61	83	86	58	82	85	64	85	88
AD/MCI	66	76	77	64	73	76	70	76	79
MCI/CN	58	73	74	54	68	71	58	79	79

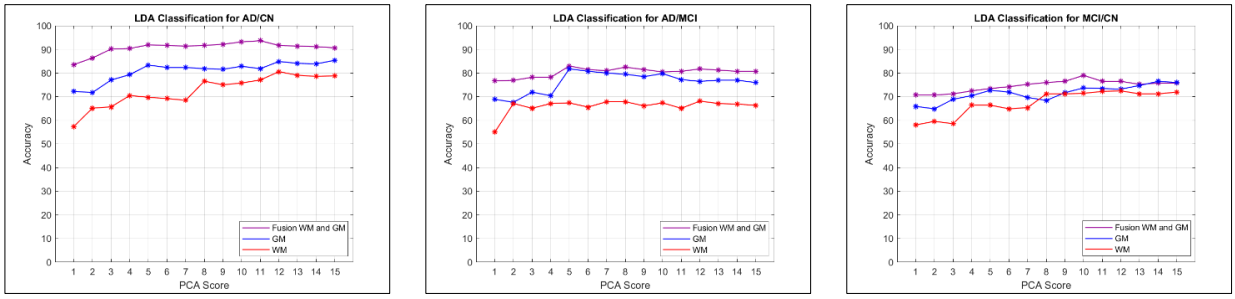

(a) (b) (c)

Figure 4. The accuracy values for the three binary classification cases were determined using white matter (red color), gray matter (blue color), and the proposed method (purple color) for 15 PCA components with LDA as the classifier.

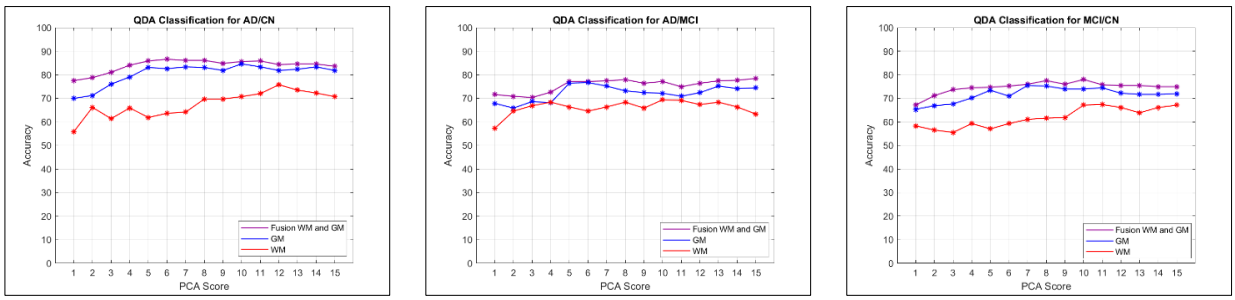

(a) (b) (c)

Figure 5. The accuracy values for the three binary classification cases were determined using white matter (red color), gray matter (blue color), and the proposed method (purple color) for 15 PCA components and using QDA as the classifier.

In AD/CN classification, the proposed method achieved an 8% and 22% increase in accuracy for gray and white matters, respectively, when using the LDA classifier. Moreover, in the QDA classifier, this increase is 3% and 25% for gray matter and white matter, respectively.

Improvements in accuracy can also be observed for the other two binary classification cases.

Table 5 shows a comparison between the results of the proposed method for gray matter and a few competing studies.

Table 5. Comparison between proposed method and competing studies

Reference	Year	Number of data			Algorithm	Study group	Performance		
		AD	MCI	CN			Spec.	Sens.	Acc.
Proposed Method	2025	200	200	200	LDA	AD/CN	88	94	91

						AD/MCI	78	85	82
						MCI/CN	67	79	73
						AD/CN	79	88.83	84.17
Zu et al. [34]	2016	83	87	61	SVM	AD/MCI	42.52	77.81	65.21
						MCI/CN	60.22	78.17	70.38
						AD/CN	79	88.83	84.17
Beheshti et al. [35]	2017	83	87	61	SVM	AD/MCI	42.52	77.81	65.21
						MCI/CN	60.22	78.17	70.38
Cui et al. [36]	2018	128	-	229	ANN+BGRU	AD/CN	92.58	86.87	89.69
						AD/CN	85.82	89.58	87.39
Vaithinathan and Parthiban [37]	2019	189	396	227	SVM+RF+KNN	AD/MCI	65.35	57.29	63.41
						MCI/CN	72.44	45.61	64.74
						AD/CN	91.68	95.47	86.68
Zhou et al. [38]	2020	116	82	142	SR-DBN+ELM	AD/MCI	80.35	85.65	72.98
						MCI/CN	88.25	79.74	91.58
						AD/CN	-	-	84
Zarei et al. [39]	2024	602	948	853	Radiometric+CNN	AD/MCI	-	-	58
						MCI/CN	-	-	72

4. Conclusion

In this study, the objective is to employ the evidence theory and Dempster-Shafer theory to enhance accuracy. This theory helps reduce uncertainty in studies related to imaging and disease diagnosis. MRI images are often subject to uncertainty due to various factors; thus, considering this uncertainty can enable a more reliable and comprehensive diagnostic process. As mentioned, MRI images inherently contain some degree of uncertainty. In this study, data obtained from white matter and gray matter were combined to minimize uncertainty and increase certainty.

The results indicate that applying this theory in the proposed method can significantly improve accuracy in various binary classification scenarios. Finally, it is noteworthy that the proposed method can be applied to different approaches for diagnosing Alzheimer's disease or other research domains, as our study and other related studies have demonstrated that this theory has performed successfully in most cases.

5. Statements & Declarations

5.1. Acknowledgments

Data collection and sharing for this project was funded by the Alzheimer's Disease Neuroimaging Initiative(ADNI) (National Institutes of Health Grant U01 AG024904) and DOD ADNI (Department of Defense award number W81XWH-12-2-0012). ADNI is funded by the National

Institute on Aging, the National Institute of Biomedical Imaging and Bioengineering, and through generous contributions from the following: AbbVie, Alzheimer’s Association; Alzheimer’s Drug Discovery Foundation; Araclon Biotech; BioClinica, Inc.; Biogen; Bristol-Myers Squibb Company; CereSpir, Inc.; Cogstate; Eisai Inc.; Elan Pharmaceuticals, Inc.; Eli Lilly and Company; EuroImmun; F. Hoffmann-La Roche Ltd and its affiliated company Genentech, Inc.; Fujirebio; GE Healthcare; IXICO Ltd.; Janssen Alzheimer Immunotherapy Research & Development, LLC.; Johnson & Johnson Pharmaceutical Research & Development LLC.; Lumosity; Lundbeck; Merck & Co., Inc.; Meso Scale Diagnostics, LLC.; NeuroRx Research; Neurotrack Technologies; Novartis Pharmaceuticals Corporation; Pfizer Inc. ; Piramal Imaging; Servier; T a k e d a Pharmaceutical Company; and

Transition Therapeutics. The Canadian Institutes of Health Research is providing funds to support ADNI clinical sites in Canada. Private sector contributions are facilitated by the Foundation for the National Institutes of Health (www.fnih.org). The grantee organization is the Northern California Institute for Research and Education, and the study is coordinated by the Alzheimer’s Therapeutic Research Institute at the University of Southern California. ADNI data are disseminated by the Laboratory for NeuroImaging at the University of Southern California.

5.2. Funding

This research was financed by a research grant from the University of Mazandaran.

5.3. Ethical statement

The authors declare that they have no conflict of interest.

6. References

[1] Rayathala, J., C, K. K., & P, V. (2022). Review on Alzheimer’s disease: past, present and future. Journal of Innovations in Applied Pharmaceutical Science (JIAPS), 28–31. doi:10.37022/jiaps.v7i1.274.

[2] Grossberg, G. T. (2003). Diagnosis and treatment of Alzheimer’s disease. Journal of Clinical Psychiatry, 64 (suppl 9), 3–6. doi:10.1212/wnl.64.12_suppl_3.s34.

[3] Edupuganti, V., Mardani, M., Vasanawala, S., & Pauly, J. (2021). Uncertainty Quantification in Deep MRI Reconstruction. IEEE Transactions on Medical Imaging, 40(1), 239–250. doi:10.1109/TMI.2020.3025065.

[4] Lohar, M. (2018). A survey on classification methods of brain MRI for Alzheimer's disease. Journal of King Saud University - Computer and Information Sciences, 7(5), 339–348.

[5] Bottero, V., Powers, D., Yalamanchi, A., Quinn, J. P., & Potashkin, J. A. (2021). Key disease mechanisms linked to alzheimer's disease in the entorhinal cortex. International Journal of Molecular Sciences, 22(8), 3915. doi:10.3390/ijms22083915.

[6] Sato, R., Kudo, K., Udo, N., Matsushima, M., Yabe, I., Yamaguchi, A., Tha, K. K., Sasaki, M., Harada, M., Matsukawa, N., Amemiya, T., Kawata, Y., Bito, Y., Ochi, H., & Shirai, T. (2022). A diagnostic index based on quantitative susceptibility mapping and voxel-based morphometry may improve early diagnosis of Alzheimer's disease. European Radiology, 32(7), 4479–4488. doi:10.1007/s00330-022-08547-3.

[7] Huang, H., Zheng, S., Yang, Z., Wu, Y., Li, Y., Qiu, J., Cheng, Y., Lin, P., Lin, Y., Guan, J., Mikulis, D. J., Zhou, T., & Wu, R. (2023). Voxel-based morphometry and a deep learning model for the diagnosis of early Alzheimer's disease based on cerebral gray matter changes. Cerebral Cortex, 33(3), 754–763. doi:10.1093/cercor/bhac099.

[8] Saha, C., Figley, C. R., Dastgheib, Z., Lithgow, B. J., & Moussavi, Z. (2024). Gray and white matter voxel-based morphometry of Alzheimer's disease with and without significant cerebrovascular pathologies. Neuroscience Insights, 19. doi:10.1177/26331055231225657.

[9] Ghasemi, J., Ghaderi, R., Karami Mollaei, M. R., & Hojjatoleslami, S. A. (2013). A novel fuzzy Dempster-Shafer inference system for brain MRI segmentation. Information Sciences, 223, 205–220. doi:10.1016/j.ins.2012.08.026.

[10] Tavakoli, F., & Ghasemi, J. (2018). Brain MRI segmentation by combining different MRI modalities using Dempster- Shafer theory. IET Image Processing, 12(8), 1322–1330. doi:10.1049/iet-ipr.2017.0473.

[11] Razi, S., Karami Mollaei, M. R., & Ghasemi, J. (2019). A novel method for classification of BCI multi-class motor imagery task based on Dempster–Shafer theory. Information Sciences, 484, 14–26. doi:10.1016/j.ins.2019.01.053.

[12] Ray, D., Majumder, D. D., & Das, A. (2010). Synergistic Study of Alzheimer Diseased Brain MRI with PET and SPECT Images using Shape based Registration and Fuzzy-Dempster Shafer Evidence Accumulation Model. International Journal of Computer Applications, 12(7), 18–25. doi:10.5120/1691-2120.

[13] Dinov, I. D., Valentino, D., Shin, B. C., Konstantinidis, F., Hu, G., MacKenzie-Graham, A., Lee, E.-F., Shattuck, D., Ma, J., Schwartz, C., & Toga, A. W. (2006). LONI Visualization Environment. Journal of Digital Imaging, 19(2), 148–158. doi:10.1007/s10278-006-0266-8.

[14] Ding, X., Charnigo, R. J., Schmitt, F. A., Kryscio, R. J., & Abner, E. L. (2019). Evaluating trajectories of episodic memory in normal cognition and mild cognitive impairment: Results from ADNI. PLoS ONE, 14(2), 212435. doi:10.1371/journal.pone.0212435.

[15] Wyman, B. T., Harvey, D. J., Crawford, K., Bernstein, M. A., Carmichael, O., Cole, P. E., Crane, P. K., DeCarli, C., Fox, N. C., Gunter, J. L., Hill, D., Killiany, R. J., Pachai, C., Schwarz, A. J., Schuff, N., Senjem, M. L., Suhy, J., Thompson, P. M., … Weiner, M. (2012). Standardization of analysis sets for reporting results from ADNI MRI data. Alzheimer's & Dementia, 9(3), 332–337. doi:10.1016/j.jalz.2012.06.004.

[16] Sambath Kumar, S., & Nandhini, M. (2022). Automated Classification of Alzheimer's Disease Using MRI and Transfer Learning. Mobile Computing and Sustainable Informatics, Springer, Singapore. doi:10.1007/978-981-16-1866-6_47.

[17] Demšar, U., Harris, P., Brunsdon, C., Fotheringham, A. S., & McLoone, S. (2013). Principal Component Analysis on Spatial Data: An Overview. Annals of the Association of American Geographers, 103(1), 106–128. doi:10.1080/00045608.2012.689236.

[18] Sudharsan, M., & Thailambal, G. (2023). Alzheimer's disease prediction using machine learning techniques and principal component analysis (PCA). Materials Today: Proceedings, 81, 182–190. doi:10.1016/j.matpr.2021.03.061.

[19] Khedher, L., Ramírez, J., Górriz, J. M., Brahim, A., & Segovia, F. (2015). Early diagnosis of Alzheimer's disease based on partial least squares, principal component analysis and support vector machine using segmented MRI images. Neurocomputing, 151, 139–150. doi:10.1016/j.neucom.2014.09.072.

[20] Turk, M., & Pentland, A. (1991). Eigenfaces for recognition. Journal of Cognitive Neuroscience, 3(1), 71–86. doi:10.1162/jocn.1991.3.1.71.

[21] Álvarez, I., Górriz, J. M., Ramírez, J., Salas-Gonzalez, D., López, M., Puntonet, C. G., & Segovia, F. (2009). Alzheimer's diagnosis using eigenbrains and support vector machines. Electronics Letters, 45(7), 342–343. doi:10.1049/el.2009.3415.

[22] Papoulis, A. (1984). Bayes' theorem in statistics and Bayes' theorem in statistics (reexamined). Probability, random variables, and stochastic processes (2nd Ed). McGraw-Hill, New York United States.

[23] Bhagyashree, S. R., & Sheshadri, H. S. (2018). Diagnosis of Alzheimer's disease using Naive Bayesian Classifier. Neural Computing and Applications, 29(1), 123–132. doi:10.1007/s00521-016-2416-3.

[24] Han, J., Kamber, M., & Pei, J. (2011). Data Preprocessing. Data mining: Concepts and techniques (3rd Ed.). Morgan Kaufmann Series in Data Management Systems,

Burlington, United States. doi:10.1016/b978-0-12-381479-1.00003-4

[25] Srivastava, S., Gupta, M. R., & Frigyik, B. A. (2007). Bayesian quadratic discriminant analysis. Journal of Machine Learning Research, 8(6), 1277–1305.

[26] Tharwat, A. (2016). Linear vs. quadratic discriminant analysis classifier: a tutorial. International Journal of Applied Pattern Recognition, 3(2), 145. doi:10.1504/ijapr.2016.079050.

[27] Shafer, G. (1976). A mathematical theory of evidence. Princeton university press, Princeton, United States. doi:10.1515/9780691214696.

[28] Du, Y.-W., & Zhong, J.-J. (2021). Generalized combination rule for evidential reasoning approach and Dempster–Shafer theory of evidence. Information Sciences, 547, 1201–1232. doi:10.1016/j.ins.2020.07.072.

[29] Halpern, J. Y., & Fagin, R. (1992). Two views of belief: belief as generalized probability and belief as evidence. Artificial Intelligence, 54(3), 275–317. doi:10.1016/0004-3702(92)90048-3.

[30] Ashburner, J. (2007). A fast diffeomorphic image registration algorithm. NeuroImage, 38(1), 95–113. doi:10.1016/j.neuroimage.2007.07.007.

[31] Colloby, S. J., Elder, G. J., Rabee, R., O'Brien, J. T., & Taylor, J. (2016). Structural grey matter changes in the substantia innominata in Alzheimer's disease and dementia with Lewy bodies: a DARTEL-VBM study. International Journal of Geriatric Psychiatry, 32(6), 615–623. doi: 10.1002/gps.4500.

[32] Ghasemi, J., Karami Mollaei, M. R., Ghaderi, R., & Hojjatoleslami, A. (2012). Brain tissue segmentation based on spatial information fusion by Dempster-Shafer theory. Journal of Zhejiang University SCIENCE C, 13(7), 520–533. doi:10.1631/jzus.c1100288.

[33] Peng, Y., Kou, G., Chen, Z., & Shi, Y. (2004). Cross-Validation and Ensemble Analyses on Multiple-Criteria Linear Programming Classification for Credit Cardholder Behavior. Computational Science - ICCS 2004. ICCS 2004. Lecture Notes in Computer Science, vol 3039. Springer, Heidelberg, Germany. doi:10.1007/978-3-540-25944-2_120.

[34] Zu, C., Jie, B., Liu, M., Chen, S., Shen, D., Zhang, D., & the Alzheimer's Disease Neuroimaging Initiative. (2016). Label-aligned multi-task feature learning for multimodal classification of Alzheimer's disease and mild cognitive impairment. Brain Imaging and Behavior, 10(4), 1148–1159. doi:10.1007/s11682-015-9480-7.

[35] Beheshti, I., Maikusa, N., Daneshmand, M., Matsuda, H., Demirel, H., & Anbarjafari, G. (2017). Classification of Alzheimer's disease and prediction of mild cognitive impairment conversion using histogram-based analysis of patient-specific anatomical brain connectivity networks. Journal of Alzheimer's Disease, 60(1), 295–304. doi:10.3233/JAD-161080.

[36] Cui, R., Liu, M., & Li, G. (2018). Longitudinal analysis for Alzheimer's disease diagnosis using RNN. 2018 IEEE 15th International Symposium on Biomedical Imaging (ISBI 2018), 1398–1401. doi:10.1109/ISBI.2018.8363833.

[37] Vaithinathan, K., & Parthiban, L. (2019). A Novel Texture Extraction Technique with T1 Weighted MRI for the Classification of Alzheimer's Disease. Journal of Neuroscience Methods, 318, 84–99. doi:10.1016/j.jneumeth.2019.01.011.

[38] Zhou, P., Jiang, S., Yu, L., Feng, Y., Chen, C., Li, F., Liu, Y., & Huang, Z. (2021). Use of a Sparse-Response Deep Belief Network and Extreme Learning Machine to Discriminate Alzheimer's Disease, Mild Cognitive Impairment, and Normal Controls Based on Amyloid PET/MRI Images. Frontiers in Medicine, 7. doi:10.3389/fmed.2020.621204.

[39] Zarei, A., Keshavarz, A., Jafari, E., Nemati, R., Farhadi, A., Gholamrezanezhad, A., Rostami, H., & Assadi, M. (2024). Automated classification of Alzheimer's disease, mild cognitive impairment, and cognitively normal patients using 3D convolutional neural network and radiomic features from T1-weighted brain MRI: A comparative study on detection accuracy. Clinical Imaging, 115, 110301. doi:10.1016/j.clinimag.2024.110301.